Synthesis and Characterization of Ru-Doped $n = 1$ and $n = 2$ Ruddlesden−Popper Manganates

Daniel J. Gallon,[†] Peter D. Battle,*[,†] Stephen J. Blundell,[‡] Jonathan C. Burley,[†] Amalia I. Coldea,[‡] Edmund J. Cussen,[§] Matthew J. Rosseinsky,*[,§] and Christopher Steer[‡]

Inorganic Chemistry Laboratory, Oxford University, South Parks Road, Oxford OX1 3QR, U.K., Clarendon Laboratory, Oxford University, Parks Road, Oxford OX1 3PU, U.K., and Chemistry Department, Liverpool University, Liverpool L69 7ZD, U.K.

Received May 13, 2002. Revised Manuscript Received June 25, 2002

Polycrystalline samples of Sr_3MnRuO_7 and $Sr_2Mn_{0.5}Ru_{0.5}O_4$ have been synthesized and characterized by neutron diffraction, dc magnetometry, and magnetotransport measurements. They are, respectively, $n = 2$ and $n = 1$ members of the Ruddlesden−Popper (RP) $A_{n+1}B_nO_{3n+1}$ family; both have tetragonal ($I4/mmm$) symmetry and a disordered distribution of Ru and Mn over the six-coordinate sites within the perovskite layers of the RP structure. Neither compound shows long-range magnetic order at 2 K, but a spin-glass transition is observed at 16 K ($n = 1$) or 25 K ($n = 2$). In the case of the $n = 2$ compound only, the magnetic transition is accompanied by a reduction in the zero-field electrical conductivity. A maximum magnetoresistance of ∼8% in 14 T is found in both compounds.

Introduction

Following the observation of large low-field magnetoresistance in $Sr_{1.8}La_{1.2}Mn_2O_7$,[1] research into the magnetotransport properties of perovskite manganates was extended to include layered Ruddlesden−Popper (RP) manganates of general formula $A_{n+1}B_nO_{3n+1}$. The RP compounds consist of $A_nB_nO_{3n}$ perovskite-like blocks, n octahedra thick, separated by a rock-salt-like layer of composition AO (Figure 1). A large number of transition metals can occupy the B cation site within the oxide octahedra, and the electronic properties of the compound are very sensitive to the chemical composition.[2] Thus, Sr_2RuO_4 ($n = 1$) is an unusual spin-triplet p-wave superconductor,[3,4] with a strongly composition-dependent transition temperature of ∼1 K,[5,6] whereas Sr_2MnO_4 is an antiferromagnetic insulator with $T_N = 170$ K.[7] Although measurements on a flux-grown single crystal indicated that $n = 2$ $Sr_3Ru_2O_7$ is ferromagnetic below 104 K,[8] polycrystalline samples prepared by Cava et al.[9] and Ikeda et al.[10] showed a magnetization maximum, indicative of antiferromagnetic spin correlations, at ∼15 K. However, neutron diffraction[11] has shown that this maximum does not correspond to the onset of long-range magnetic order. Data collected on crystals grown by the floating zone method[12] are consistent with those collected on polycrystalline samples, emphasizing the sensitivity of the magnetic properties of this system to

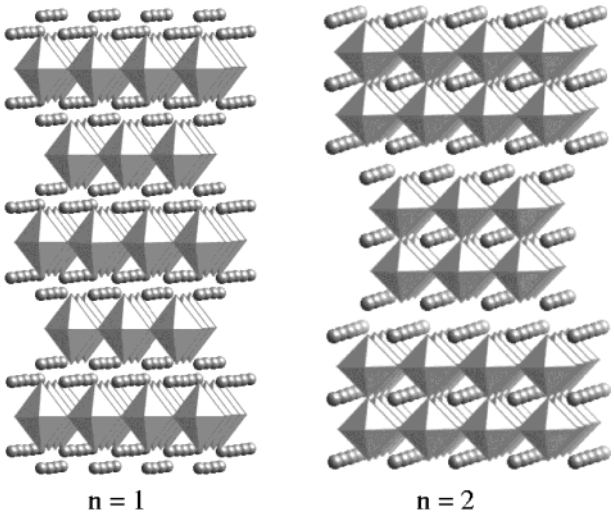

Figure 1. Crystal structures of Ruddlesden−Popper phases $n = 1$ and $n = 2$. MnO_6 octahedra are shaded; circles represent Sr cations.

* To whom correspondence should be addressed. E-mail: peter.battle@chem.ox.ac.uk or m.j.rosseinsky@liverpool.ac.uk.
† Inorganic Chemistry Laboratory, Oxford University.
‡ Clarendon Laboratory, Oxford University.
§ Liverpool University.

(1) Moritomo, Y.; Asamitsu, A.; Kuwahara, H.; Tokura, Y. *Nature* **1996**, *380*, 141.
(2) Battle, P. D.; Rosseinsky, M. J. *Curr. Opin. Solid State Mater. Sci.* **1999**, *4*, 163.
(3) Ishida, K.; Mukuda, H.; Kitaoka, Y.; Asayama, K.; Mao, Z. Q.; Mori, Y.; Maeno, Y. *Nature* **1998**, *396*, 658.
(4) Luke, G. M.; Fudamoto, Y.; Kojima, K. M.; Larkin, M. I.; Merrin, J.; Nachumi, B.; Uemura, Y. J.; Maeno, Y.; Mao, Z. Q.; Mori, Y.; Nakamura, H.; Sigrist, M. *Nature* **1998**, *394*, 558.
(5) Maeno, Y.; Hashimoto, H.; Yoshida, K.; Nishizaki, S.; Fujita, T.; Bednorz, J. G.; Lichtenberg, F. *Nature* **1994**, *372*, 532.
(6) Mackenzie, A. P.; Haselwimmer, R. K. W.; Tyler, A. W.; Lonzarich, G. G.; Mori, Y.; Nishizaki, S.; Maeno, Y. *Phys. Rev. Lett.* **1998**, *80*, 161.
(7) Bouloux, J. C.; Soubeyroux, J. L.; le-Flem, G.; Hagenmuller, P. *J. Solid State Chem.* **1981**, *38*, 34.
(8) Cao, G.; McCall, S.; Crow, J. E. *Phys. Rev. B* **1997**, *55*, R672.
(9) Cava, R. J.; Zandbergen, H. W.; Krajewski, J. J.; Peck, W. F., Jr.; Batlogg, B.; Carter, S.; Fleming, R. M.; Zhou, O.; Rupp, L. W., Jr. *J. Solid State Chem.* **1995**, *116*, 141.
(10) Ikeda, S.; Maeno, Y.; Nohara, M.; Fujita, T. *Physica C* **1996**, *263*, 558.
(11) Huang, Q.; Lynn, J. W.; Erwin, R. W.; Jarupatrakorn, J.; Cava, R. J. *Phys. Rev. B* **1998**, *58*, 8515.
(12) Ikeda, S.; Maeno, Y. *Physica B* **1999**, *259−261*, 947.

10.1021/cm021202s CCC: $22.00
Published on Web 08/09/2002

the method of synthesis. The conductivity of $Sr_3Ru_2O_7$ is best described in terms of an exchange-enhanced Fermi liquid,[13,14] and it is worth noting that a magnetic field has a large effect on the ground state.[15] In contrast, $Sr_3Mn_2O_7$ is an antiferromagnetic insulator with T_N = 160 K.[16] Interest in mixed Mn/Ru phases was aroused by the observation that doping insulating, charge-ordered $n = \infty$ (i.e., perovskite) manganates with low concentrations of Ru can induce ferromagnetism and metalicity.[17−19] Ganguly et al. have subsequently shown[20] that the introduction of Ru into $La_{0.5}Sr_{1.5}MnO_4$ and $LaSr_2Mn_2O_7$ also causes an increase in magnetization while destroying charge ordering; they noted that Ru was less soluble in the $n = 1$ or 2 materials than in the $n = \infty$ perovskites. Sharma et al.[21] were able to prepare the La-free phase Sr_3MnRuO_7 and found indications of a ferromagnetic transition coincident with an insulator−metal transition at approximately 66 K. However, the neutron diffraction and magnetometry data presented below demonstrate that although the magnetic susceptibilities of Sr_3MnRuO_7 and the analogous n =1 phase $Sr_2Mn_{0.5}Ru_{0.5}O_4$ show complex behavior as a function of temperature, neither compound exhibits long-range magnetic order at 2 K; the magnetometry data must be interpreted in terms of spin-glass or cluster-glass behavior.

Experimental Section

We attempted to synthesize $n = 1$ $Sr_{2-x}La_xMn_{0.5}Ru_{0.5}O_4$ and $n = 2$ $Sr_{3-x}La_xMnRuO_7$ for selected compositions in the range $0 \le x \le 1$. However, our attempts at La substitution were unsuccessful in both the $n = 1$ and $n = 2$ RP systems, and only the Sr-rich end members will be discussed below. The stoichiometric quantities of dried RuO_2, $SrCO_3$, and MnO_2 required to prepare 1 g aliquots of each composition were weighed out accurately, ground together, and fired at 800 °C. They were then pressed into pellets of 13 mm diameter before being fired at higher temperatures. $Sr_2Mn_{0.5}Ru_{0.5}O_4$ was fired at 1000 (1 day) and 1250 (4 days) °C. Sr_3MnRuO_7 was fired at 1000 (1 day), 1200 (2 days), 1300 (4 days), and 1350 (9 days) °C, with intermediate grinding and repelletization. The progress of the reaction was monitored by X-ray powder diffraction, and firing was halted when the pattern was consistent with the presence of a single RP phase only, and when the fwhm's of the 0 0 2 reflection ($n = 1$) and the 0 0 10 reflection ($n = 2$) were comparable to the characteristic peak width of the diffractometer (Siemens D5000 operating with Cu $K\alpha_1$ radiation). Three pellets of each composition were then mixed together, after Rietveld refinement of X-ray data and analysis of magnetic susceptibility measurements had demonstrated that the aliquots were identical within experimental error.

Table 1. Structural Parameters of $Sr_2Mn_{0.5}Ru_{0.5}O_4$ at 298 and 2 K[a]

		298 K	2 K
	a/Å	3.8785(1)	3.86079(9)
	c/Å	12.5057(6)	12.5131(4)
	V/Å^3	188.1	186.5
Sr	z	0.3558(1)	0.3559(1)
	U_{11}/Å^2	0.0058(6)	−0.0004(5)
	U_{33}/Å^2	0.0038(8)	0.0023(7)
Mn/Ru	U_{11}/Å^2	0.003(3)	0.003(6)
	U_{33}/Å^2	0.045(7)	0.031(6)
O1	z	0.1590(2)	0.1590(1)
	U_{11}/Å^2	0.0116(7)	0.0053(6)
	U_{33}/Å^2	0.007(1)	0.002(1)
O2	U_{11}/Å^2	0.002(1)	−0.0015(9)
	U_{22}/Å^2	0.013(1)	0.007(1)
	U_{33}/Å^2	0.007(1)	0.0060(8)

[a] Space group $I4/mmm$. Sr on 4e 0 0 z, Mn/Ru on 2a 0 0 0, O1 on 4e 0 0 z, O2 on 4c 0.5 0 0. 298 K, R_{wp} = 5.59%, χ^2 = 1.214; 2 K, R_{wp} = 5.16%, χ^2 = 2.324. λ = 1.59452 Å.

These consolidated samples (~3 g each) were then studied by neutron powder diffraction on the D2b diffractometer, ILL Grenoble (λ = 1.5945 Å). Data were collected over the angular range $0 \le 2\theta/\text{deg} \le 150$ at room temperature and 2 K with the sample contained in a V can which was mounted in a standard ILL cryostat. Mn K-edge XANES was performed on these samples, along with a number of standards containing Mn in a known oxidation state, on station 7.1 at the SRS, Daresbury Laboratory. The position of the absorption edge was defined by the point of inflection in each spectrum.

Magnetic susceptibility measurements were performed using a Quantum Design SQUID magnetometer. The dc molar magnetic susceptibility of each sample was measured as a function of temperature in the range $5 \le T/\text{K} \le 300$; data were collected on warming in fields of 100 and 1000 Oe after the sample was cooled in zero applied field (ZFC) and in the measuring field (FC). The field dependence of the magnetization was studied over the range $-50 \le \text{H/kOe} \le 50$ at a number of temperatures, selected after inspection of the temperature dependence of the susceptibility.

Magnetoresistance measurements were made, using standard four-probe geometry, at a range of temperatures and field strengths on bars of approximate dimensions 5 × 2 × 2 mm which had been sintered at 1250 °C ($Sr_2Mn_{0.5}Ru_{0.5}O_4$) or 1350 °C (Sr_3MnRuO_7). The resistivity of the n = 1 phase was immeasurably large below 25 K.

Selected-area electron diffraction patterns were recorded using a JEOL 2000FX transmission electron microscope with a double-tilting goniometer stage (±30°). The finely ground sample was suspended in hexane, and then mounted on lacy carbon-coated grids.

Results

The Bragg peaks in the X-ray and neutron powder diffraction patterns collected on $Sr_2Mn_{0.5}Ru_{0.5}O_4$ could be indexed in the tetragonal space group $I4/mmm$ (No. 139). Rietveld analysis,[22] performed using the GSAS software package,[23] of the neutron data collected at both room temperature and 2 K proceeded smoothly when the structure was assumed to be that of a simple $n = 1$ RP phase. The resultant structural parameters and bond lengths are presented in Tables 1 and 2, respectively. Previous studies of RP phases have shown[24,25]

(13) Perry, R. S.; Galvin, L. M.; Grigera, S. A.; Capogna, L.; Schofield, A. J.; Mackenzie, A. P.; Chiao, M.; Julian, S. R.; Ikeda, S. I.; Nakatsuji, S.; Maeno, Y.; Pfleiderer, C. *Phys. Rev. Lett.* **2001**, *86*, 2661.
(14) Ikeda, S. I.; Maeno, Y.; Nakatsuji, S.; Kosaka, M.; Uwatoko, Y. *Phys. Rev. B* **2000**, *62*, R6089.
(15) Grigera, S. A.; Perry, R. S.; Schofield, A. J.; Chiao, M.; Julian, S. R.; Lonzarich, G. G.; Ikeda, S. I.; Maeno, Y.; Millis, A. J.; Mackenzie, A. P. *Science* **2001**, *294*, 329.
(16) Mitchell, J. F.; Millburn, J. E.; Medarde, M.; Short, S.; Jorgensen, J. D.; Fernández-Díaz, M. T. *J. Solid State Chem.* **1998**, *141*, 599.
(17) Martin, C.; Maignan, A.; Hervieu, M.; Raveau, B.; Hejtmanek, J. *Eur. Phys. J. B* **2000**, *16*, 469.
(18) Raveau, B.; Maignan, A.; Martin, C.; Mahendiran, R.; Hervieu, M. *J. Solid State Chem.* **2000**, *151*, 330.
(19) Vanitha, P. V.; Arulraj, A.; Raju, A. R.; Rao, C. N. R. *C. R. Acad. Sci. II* **1999**, *2*, 595.
(20) Ganguly, R.; Martin, C.; Maignan, A.; Hervieu, M.; Raveau, B. *Solid State Commun.* **2001**, *120*, 363.
(21) Sharma, I. B.; Magorta, S. K. *J. Alloys Compd.* **1999**, *284*, 18.
(22) Rietveld, H. M. *J. Appl. Crystallogr.* **1969**, *2*, 65.
(23) Larson, A. C.; von-Dreele, R. B. *General Structure Analysis System (GSAS)*; Report LAUR 86-748, Los Alamos National Laboratories: Los Alamos, NM, 1990.
(24) Battle, P. D.; Green, M. A.; Laskey, N. S.; Millburn, J. E.; Radaelli, P. G.; Rosseinsky, M. J.; Sullivan, S. P.; Vente, J. F. *Phys. Rev. B* **1996**, *54*, 15967.

Table 2. Selected Bond Lengths (Å) in $Sr_2Mn_{0.5}Ru_{0.5}O_4$ at 298 and 2 K

	298 K	2 K		298 K	2 K
Sr1−O1, ×1	2.461(2)	2.464(2)	Mn/Ru−O1, ×2	1.988(2)	1.989(2)
Sr1−O1, ×4	2.7488(2)	2.7363(2)	Mn/Ru−O2, ×4	1.93928(6)	1.93039(5)
Sr1−O2, ×4	2.648(1)	2.6416(9)			

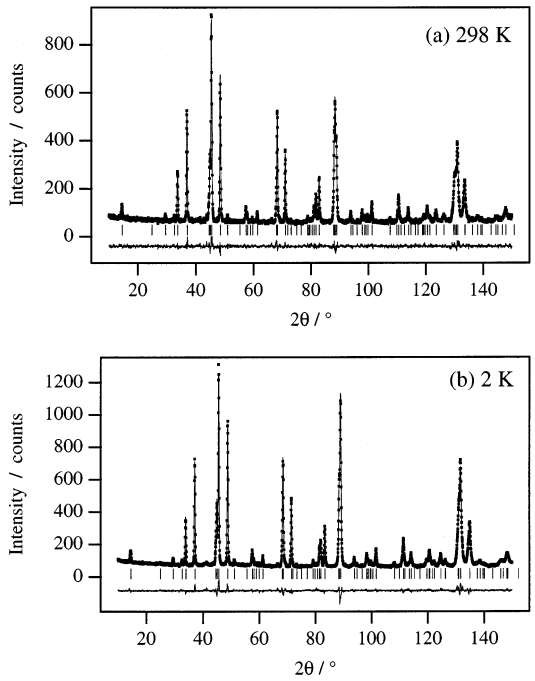

Figure 2. Observed (●), calculated (—), and difference neutron powder diffraction profiles for $Sr_2Mn_{0.5}Ru_{0.5}O_4$ at (a) 298 K and (b) 2 K. Tick marks indicate positions of allowed reflections.

that apparently monophasic samples may contain at least two compositions having the same value of n. The best diagnostic of this is the increase in the fwhm of a 0 0 l reflection which usually occurs on cooling of a multiphasic sample. No significant broadening of the 0 0 2 reflection was observed on cooling, showing that the sample contained only one $n = 1$ phase (fwhm of 0 0 2; 0.35(2)° at 298 K, 0.41(2)° at 2 K). Trial refinements found no evidence for a significant vacancy concentration on the anion sublattice. The observed and calculated diffraction profiles are plotted in Figure 2. The unit cell volume contracts on cooling, as expected, but in an anisotropic manner; the structure contracts in the xy plane, but expands along z. The displacement parameters of the Mn/Ru cation, O1, and O2 also show significant anisotropy. The former has an enhanced value of U_{33}, and at 298 K O1 and O2 have high values of U_{11} and U_{22}, respectively, which both reduce by ∼50% on cooling to 2 K.

A small (approximately 1% by mass) perovskite impurity was observed in the neutron diffraction pattern collected on Sr_3MnRuO_7, and the affected areas were excluded from the Rietveld analysis of the data. Otherwise, the data could be accounted for in space group $I4/mmm$ with a simple $n = 2$ RP structure. There was no evidence of an additional contribution from long-range magnetic order in the low-temperature neutron diffraction pattern, and the data were therefore fitted using a model consisting of nuclear scattering only. The fwhm of the 0 0 10 reflection from Sr_3MnRuO_7 did not change significantly on cooling (0.327(4)° at 290 K, 0.336(4)° at 2 K), thus indicating that our sample contains only one $n = 2$ RP phase. Rietveld refinement of the occupancy of the oxygen sites revealed no significant deviation from the ideal stoichiometry. The refined structural parameters are listed in Table 3, with the corresponding bond lengths presented in Table 4. The observed and calculated diffraction profiles are plotted in Figure 3. As in the case of $Sr_2Mn_{0.5}Ru_{0.5}O_4$, the displacement parameters of the anions and the Mn/Ru site are strongly anisotropic at room temperature, but less so at 2 K.

Electron diffraction patterns taken down the [0 0 1] zone axis of both samples (Figure 4) were consistent with the structural models described in Tables 1 and 3; there was no evidence of a supercell. This indicates that there is no cation ordering on the B site, even over a distance scale much shorter than that sampled in the neutron diffraction experiments described above.

In the temperature range $180 < T/K < 300$, the molar magnetic susceptibility of $Sr_2Mn_{0.5}Ru_{0.5}O_4$, measured (Figure 5) in 100 Oe, can be fitted to a Curie−Weiss law (Table 5) with parameters which are characteristic of a weakly interacting array of Mn^{4+} and Ru^{4+} cations.

Table 3. Structural Parameters of Sr_3MnRuO_7 at 290, 60, and 2 K[a]

		290 K	60 K	2 K
	a/Å	3.90450(4)	3.89558(5)	3.89507(5)
	c/Å	20.1274(3)	20.1047(3)	20.1047(3)
	V/Å^3	306.8	305.1	305.0
Sr1	U_{11}/Å^2	0.0096(9)	0.0032(7)	0.0029(7)
	U_{33}/Å^2	0.008(1)	0.003(1)	0.005(1)
Sr2	z	0.31638(8)	0.31629(7)	0.31628(7)
	U_{11}/Å^2	0.0076(6)	0.0037(4)	0.0037(5)
	U_{33}/Å^2	0.0079(7)	0.0053(6)	0.0040(6)
Mn/Ru	z	0.0964(3)	0.0970(3)	0.0961(2)
	U_{11}/Å^2	0.007(1)	0.009(1)	0.011(1)
	U_{33}/Å^2	0.011(2)	0.009(2)	0.004(2)
O1	z	0.09630(7)	0.09618(6)	0.09620(6)
	U_{11}/Å^2	0.0084(8)	0.0042(7)	0.0042(7)
	U_{22}/Å^2	0.0074(8)	0.0052(7)	0.0060(7)
	U_{33}/Å^2	0.0115(5)	0.0062(5)	0.0046(5)
O2	z	0.19391(9)	0.19408(8)	0.19396(8)
	U_{11}/Å^2	0.0108(7)	0.0051(6)	0.0045(6)
	U_{33}/Å^2	0.006(1)	0.005(1)	0.005(1)
O3	U_{11}/Å^2	0.012(1)	0.0078(9)	0.0065(9)
	U_{33}/Å^2	0.008(1)	0.005(1)	0.008(1)

[a] Sr1 0 0 0.5, Sr2 0 0 z_1, Mn/Ru 0 0 z_2, O1 0 0.5 z_3, O2 0 0 z_4, O3 0 0 0. 290 K, $R_{wp} = 4.59\%$, $\chi^2 = 1.921$; 60 K, $R_{wp} = 4.31\%$, $\chi^2 = 1.672$; 2 K, $R_{wp} = 4.50\%$, $\chi^2 = 1.827$. $\lambda = 1.594373$ Å.

Table 4. Selected Bond Lengths (Å) in Sr_3MnRuO_7 at 298, 60, and 2 K

	290 K	60 K	2 K
Sr1−O1, ×8	2.751(1)	2.7447(9)	2.7448(9)
Sr1−O3, ×4	2.76090(3)	2.75459(4)	2.75423(4)
Sr2−O1, ×4	2.627(2)	2.625(1)	2.625(1)
Sr2−O2, ×1	2.465(2)	2.457(2)	2.459(2)
Sr2−O2, ×4	2.7686(2)	2.7625(2)	2.7619(2)
Mn−O1, ×4	1.95225(2)	1.94786(6)	1.94754(3)
Mn−O2, ×1	1.962(6)	1.951(6)	1.967(6)
Mn−O3, ×1	1.941(6)	1.950(6)	1.933(6)

(25) Battle, P. D.; Cox, D. E.; Green, M. A.; Millburn, J. E.; Spring, L. E.; Radaelli, P. G.; Rosseinsky, M. J.; Vente, J. F. *Chem. Mater.* **1997**, *9*, 1042.

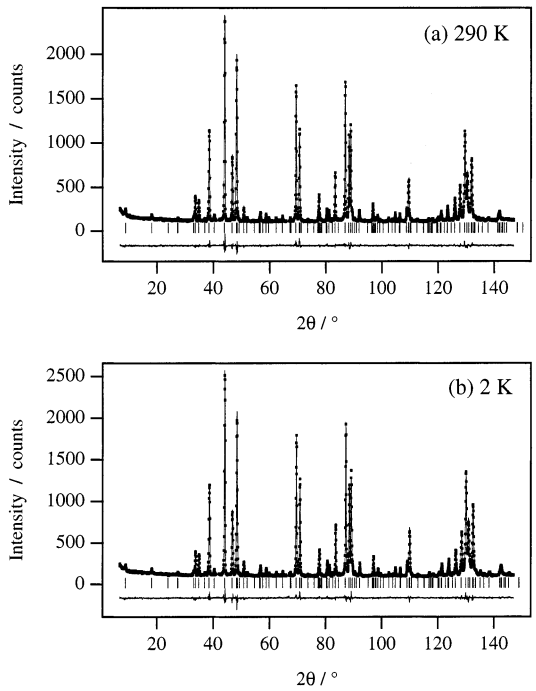

Figure 3. Observed (●), calculated (—), and difference neutron powder diffraction profiles for Sr_3MnRuO_7 at (a) 290 K and (b) 2 K. Tick marks indicate positions of allowed reflections.

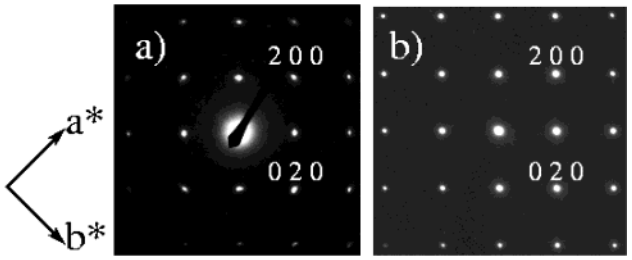

Figure 4. [0 0 1] electron diffraction patterns of (a) $Sr_2Mn_{0.5}Ru_{0.5}O_4$ and (b) Sr_3MnRuO_7.

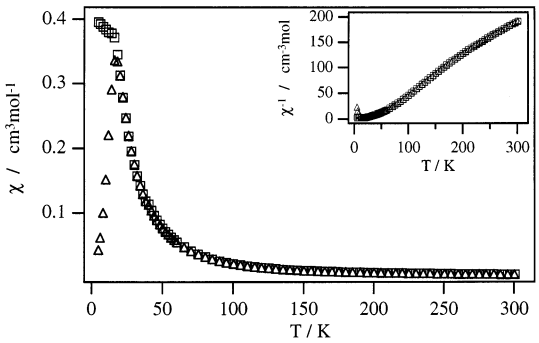

Figure 5. Temperature dependence of (△) zero-field-cooled and (□) field-cooled molar magnetic susceptibility and reciprocal molar susceptibility (inset) of $Sr_2Mn_{0.5}Ru_{0.5}O_4$ measured in 100 Oe.

However, on cooling below ~200 K, the susceptibility begins to increase more rapidly than would be predicted by the Curie−Weiss law. This is demonstrated by the nonlinear temperature dependence of the inverse susceptibility. The ZFC susceptibility shows a maximum at 16 K, although the FC susceptibility continues to rise slowly on further cooling. Qualitatively similar behavior is observed in the data collected in 1000 Oe, although the susceptibility is field dependent below ~80 K. These results suggest that $Sr_2Mn_{0.5}Ru_{0.5}O_4$ is a cluster glass

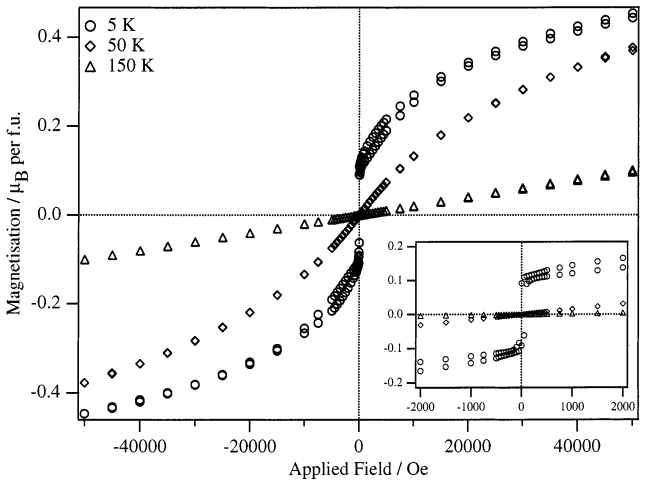

Figure 6. Magnetization (per formula unit) of $Sr_2Mn_{0.5}Ru_{0.5}O_4$ as a function of applied field and temperature. The low-field behavior is detailed in the inset.

Table 5. Curie−Weiss Parameters for $Sr_2Mn_{0.5}Ru_{0.5}O_4$ as a Function of Applied Field

	100 Oe	1000 Oe
C/cm^3 mol^{-1} K	1.51(1)	1.59(1)
θ/K	6(1)	9(1)
range fitted/K	180−300	180−300

Table 6. Curie−Weiss Parameters for Sr_3MnRuO_7 as a Function of Applied Field

	100 Oe	1000 Oe	50000 Oe
C/cm^3 mol^{-1} K	2.90(3)	3.19(1)	3.36(2)
θ/K	41(3)	29(1)	17.5(1)
range fitted/K	230−301	230−300	230−300

below 16 K, a conclusion which is consistent with the absence of magnetic Bragg scattering from the neutron diffraction data collected at 2 K. The field dependence of the magnetization of $Sr_2Mn_{0.5}Ru_{0.5}O_4$ (Figure 6) is nonlinear at 50 K and more markedly so at 5 K. However, the maximum magnetization increases only slightly on cooling to the lower temperature.

Although the Curie−Weiss law can be used (Table 6) to model Sr_3MnRuO_7 as a localized-electron Mn^{4+}/Ru^{4+} compound above 230 K, the $n = 2$ material shows a more complex magnetic behavior at low temperatures. The ZFC and FC molar susceptibilities measured in 100 Oe rise rapidly below 200 K and show a broad maximum at approximately 90 K; hysteresis is apparent below this maximum, and a sharp transition is present in both datasets at 25 K (Figure 7). On increasing the applied field, the transition at 90 K becomes less apparent and no hysteresis is observed above the transition at 25 K. The nonlinear field dependence of the magnetization (Figure 8) shows that our sample cannot be described as a Curie−Weiss paramagnet for temperatures ≤150 K.

The conductivity data in Figure 9 show that $Sr_2Mn_{0.5}Ru_{0.5}O_4$ is an insulator over the temperature range studied, with a magnetoresistance that increases with decreasing temperature, reaching a value of ~8% in 14 T at 50 K (Figure 10). Although less resistive, Sr_3MnRuO_7 (Figure 11) also showed insulator characteristics above approximately 25 K, but the resistivity falls sharply on cooling below this temperature. This compound showed (Figure 12) a maximum magnetoresistance of ~8% in 14 T at between 50 and 75 K.

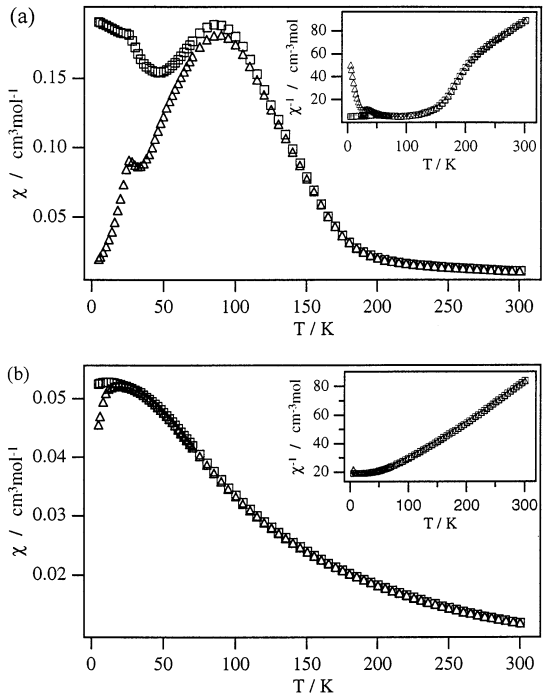

Figure 7. Temperature dependence of (△) zero-field-cooled and (□) field-cooled molar magnetic susceptibility and reciprocal molar susceptibility (inset) of Sr_3MnRuO_7 measured in (a) 100 Oe and (b) 50 kOe.

Comparison of XANES data collected on our samples with those collected on the chosen standards (Table 7) shows that at room temperature both compounds exhibit manganese oxidation states somewhere between Mn(III) and Mn(IV). The difference (1.3 eV) between the edge position in the two Mn(IV) standards, presumably stemming from differences in the local structural environment, is greater than the difference (1.1 eV) between Mn(III) in La_2GaMnO_6 and Mn(IV) in $SrMnO_3$. We therefore choose not to rely on these data to assign cation oxidation states definitively.

Discussion

Our neutron and electron diffraction data show that both the $n = 1$ and $n = 2$ compounds adopt an undistorted Ruddlesden−Popper structure with the tetragonal space group $I4/mmm$. The electron diffraction patterns provide no evidence of unit cell expansion, thus eliminating the possibility of cation ordering over distances too short to give rise to coherent diffraction effects in the neutron experiments.[26] This lack of ordering is not surprising in view of the similarity of the charges and radii of the transition-metal cations present. Investigation of the fwhm of selected neutron diffraction peaks revealed no evidence of the type of phase separation which has been observed in other RP systems,[2] and we therefore assume that the properties described above are those of the bulk phases having the nominal stoichiometric compositions $Sr_2Mn_{0.5}Ru_{0.5}O_4$ and Sr_3MnRuO_7. To interpret our data in any depth, we must first assign oxidation states to the Mn and Ru cations. In view of the failure of XANES to provide a clear resolution of this issue, we shall turn to the magnetic data shown in Figures 5 and 7, and the derived parameters given in Tables 5 and 6. The high-temperature Curie constants predicted for a 1:1 mixture of Mn^{4+} and low-spin Ru^{4+} are 1.44 and 2.87 emu mol^{-1} for $n = 1$ and $n = 2$, respectively; the corresponding values for a 1:1 mixture of high-spin Mn^{3+} and Ru^{5+} are 2.43 and 4.88. The tabulated values of 1.51 and 2.90 lead us firmly toward the former cation combination in both cases. In that case, $Sr_2Mn_{0.5}Ru_{0.5}O_4$ might be expected to have unit cell parameters midway between those of Sr_2MnO_4 and Sr_2RuO_4, in accordance with

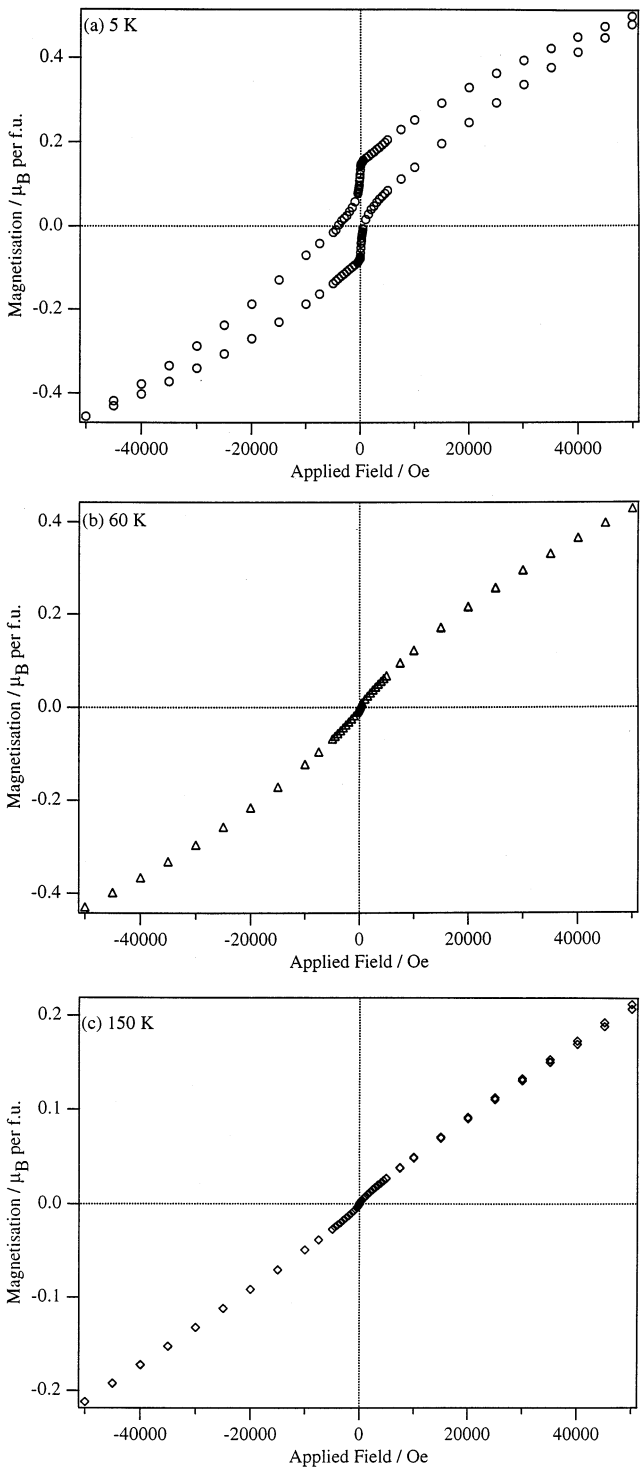

Figure 8. Magnetization (per formula unit) of Sr_3MnRuO_7 as a function of applied field and temperature: (a) 5 K, (b) 60 K, and (c) 150 K.

(26) Burley, J. C.; Battle, P. D.; Gallon, D. J.; Sloan, J.; Grey, C. P.; Rosseinsky, M. J. *J. Am. Chem. Soc.* **2002**, *124*, 620.

Table 7. Mn K-Edge Absorption Energies Determined by XANES

	La_2GaMnO_6 (Mn(III))	$SrMnO_3$ (Mn(IV))	$BaMnO_3$ (Mn(IV))	$Sr_2Mn_{0.5}Ru_{0.5}O_4$	Sr_3MnRuO_7
edge position/eV	6550.1 (2)	6552.2(3)	6553.5(1)	6551.8(4)	6550.7(4)

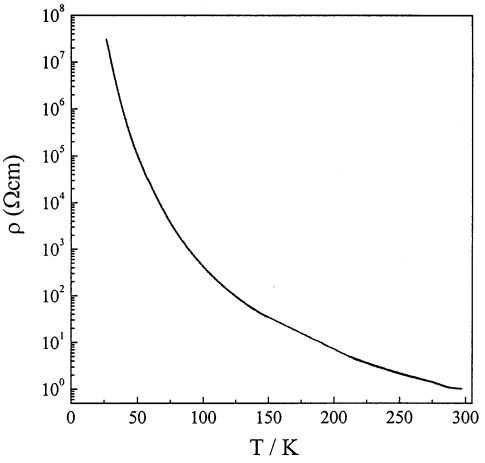

Figure 9. Resistivity of $Sr_2Mn_{0.5}Ru_{0.5}O_4$ as a function of temperature.

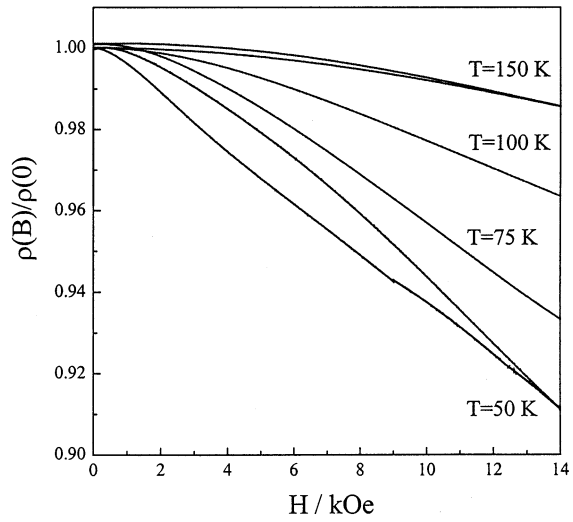

Figure 10. Magnetoresistance of $Sr_2Mn_{0.5}Ru_{0.5}O_4$ as a function of magnetic field and temperature.

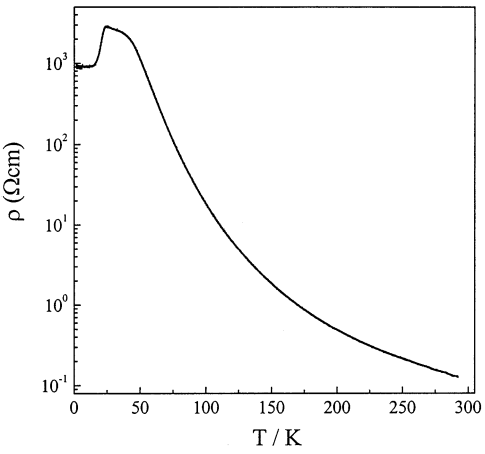

Figure 11. Resistivity of Sr_3MnRuO_7 as a function of temperature.

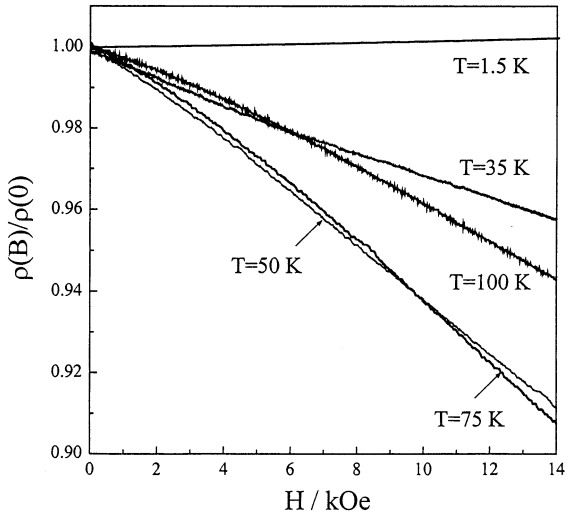

Figure 12. Magnetoresistance of Sr_3MnRuO_7 as a function of magnetic field and temperature.

Vegard's law. In fact, the unit cell parameter *a* of $Sr_2Mn_{0.5}Ru_{0.5}O_4$ is slightly larger than that of Sr_2RuO_4, despite the introduction of the nominally smaller first-row metal, and the unit cell parameter *c* is reduced to a value which is intermediate between those reported in two previous investigations[7,27] of the other end member, Sr_2MnO_4. The nonlinear composition dependence of the unit cell parameters is a consequence of changes in the electronic structure. Sr_2RuO_4 is nonmagnetic and metallic, with four electrons occupying the lower portion of a band of allowed states formed by the overlap of degenerate, narrow d_{xz} and d_{yz} orbitals and a relatively broad d_{xy} band.[28] The layered nature of the crystal structure is responsible for the anisotropy in the energy width of the levels, and the empty states at the top of the band have a large component of d_{xy} character. In contrast, Sr_2MnO_4 is an antiferromagnetic insulator with a localized, $S = 3/2$ t_{2g}^3 electron configuration on the Mn^{4+} cations. When Mn^{4+} is substituted for Ru^{4+} in Sr_2RuO_4, there is an increase in electron density in the *xy* plane because the Ru^{4+} electrons localize, adopting a $(d_{xz}, d_{yz})^3$ d_{xy}^1 configuration, and because the Mn^{4+} cation itself has a half-filled d_{xy} orbital. This relative increase in *xy* electron density counters the decrease in mean cation radius such that the required overall reduction in unit cell volume occurs almost entirely by virtue of a large contraction along the *c* axis. As a consequence of the anisotropic change, the room-temperature value of the octahedral distortion parameter $D = \langle$mean axial bond length$\rangle/\langle$equatorial bond length$\rangle$[16] decreases from 1.065 in the case of Sr_2RuO_4 to 1.025 in the case of $Sr_2Mn_{0.5}Ru_{0.5}O_4$. The mean Sr−O bond length is essentially unchanged (2.687 vs 2.672 Å), and the only remarkable atomic parameters are the U_{11} component of the displacement parameter of the axial oxide ion (O1) and the U_{22} displacement parameter of the in-plane oxide ion (O2); both of these displacements are perpendicular to the *z* axis and to the Mn/Ru−O

(27) Tezuka, K.; Inamura, M.; Hinatsu, Y.; Shimojo, Y.; Morii, Y. *J. Solid State Chem.* **1999**, *145*, 705.
(28) Nakatsuji, S.; Maeno, Y. *Phys. Rev. B* **2000**, *62*, 6458.

bond. It is likely that these atoms are subject to static displacements to accommodate the different coordination requirements of Mn^{4+} and Ru^{4+}. The unit cell volume of $Sr_2Mn_{0.5}Ru_{0.5}O_4$ contracts on cooling, but again anisotropic effects are seen; although the unit cell parameter *a* decreases, *c* increases and the value of *D* increases to 1.030. The absolute contraction in *a* is double that observed on cooling of Sr_2RuO_4. It has been argued[29] in the case of $Sr_3Ru_2O_7$ that the electron distribution in the t_{2g} orbitals of Ru^{4+}, and the extent of spin-pairing, is temperature dependent and the nonlinear behavior of χ^{-1}:*T* (Figure 4) suggests that a similar redistribution of charge might occur in $Sr_2Mn_{0.5}Ru_{0.5}O_4$. The contraction in the *xy* plane is accompanied by a reduction (~50%) in the value of both O1(U_{11}) and O2(U_{22}), although they remain higher than the other displacement parameters. We conclude either that the modified site geometry accommodates the mixed Ru/Mn distribution with less anion disorder or that the disorder has a dynamic component which decreases on cooling. The additional destabilization of the transition-metal d_{xy} orbitals brought about by the contraction in the *xy* plane can, in the case of Ru^{4+} (but not Mn^{4+}), be thought of as an increased Jahn−Teller effect, with the increase causing a shift in the balance between static and dynamic anion displacements.

The above discussion of $Sr_2Mn_{0.5}Ru_{0.5}O_4$ is largely a comparison with Sr_2RuO_4 for the simple reason that the latter compound has been characterized more fully than Sr_2MnO_4. In contrast, reliable structural data are available on both $Sr_3Mn_2O_7$[16] and $Sr_3Ru_2O_7$,[30] although a direct comparison with Sr_3MnRuO_7 is hindered by the fact that the Ru end member adopts an orthorhombic variant of the $n = 2$ RP structure. However, it is clear that, as in the case of the $n = 1$ system, the unit cell parameter *a* of the mixed Mn/Ru phase (Table 3) is larger than the corresponding distance in either end member (in the case of orthorhombic $Sr_3Ru_2O_7$, comparison is made with the value of $a_{ortho}/\sqrt{2}$ ($\approx b_{ortho}/\sqrt{2}$)), whereas the unit cell parameter *c* lies much closer to the value of 20.1289 Å observed in $Sr_3Mn_2O_7$ than it does to that of 20.725 Å in $Sr_3Ru_2O_7$. Consequently, the octahedral distortion parameter takes a value $D = 1.000$ for Sr_3MnRuO_7, compared to values of 1.015 and 1.034, respectively, in the Mn and Ru end members. The composition dependence of the unit cell parameters can again be explained in terms of a transition from a metallic, delocalized Ru electron system in $Sr_3Ru_2O_7$ to a localized $S = 1$ system, carrying a magnetic moment, in the Sr_3MnRuO_7 sample. Static anion displacements, required to accommodate the disordered Mn/Ru distribution, were found for both O1 and O2 in $n = 1$ $Sr_2Mn_{0.5}Ru_{0.5}O_4$, and they occur at both the axial site on the outer edge of the double layer (O2(U_{11})) and in the Mn/Ru sheets (O1(U_{33})) of $n = 2$ Sr_3MnRuO_7; the displacements are again perpendicular to the Mn/Ru−O bonds. The precision of our data is sufficient to show that the Mn/Ru−O1 bonds contract on cooling, but is insufficient to permit us to draw any meaningful conclusion about the temperature dependence of the axial Mn/Ru−O2/O3 distances. This imprecision arises largely because the mean neutron scattering length of the Mn/Ru site is low. However, the distance O2−O3, essentially the total axial length of the Mn/RuO_6 octahedra parallel to [001], is better defined and can be determined to be 3.903(2), 3.902(2), and 3.900(2) Å at 290, 60, and 2 K, respectively. The constancy of this value, together with the contraction of the equatorial Mn−O1 bonds, results in a small increase in the value of *D* on cooling. This in turn would favor a slight reduction in electron density in the *xy* plane and an increased occupancy of orbitals having a component along [001]. We shall return to this point below.

The temperature dependence of the magnetic susceptibility of $Sr_2Mn_{0.5}Ru_{0.5}O_4$ above ~50 K (Figure 5) suggests that, overall, the short-range interactions in this material are predominantly ferromagnetic. However, the observation of both a susceptibility maximum at 16 K and hysteresis between the ZFC and FC data suggests that at low temperatures this compound is a spin glass or a cluster glass. The field dependence of the magnetization suggests that the sample is paramagnetic at 150 K, that local interatomic coupling is apparent at 50 K, and that spin-glass freezing occurs in the temperature range $5 \leq T/K \leq 50$. This is in accord with the neutron diffraction data collected at 2 K, which show no evidence of magnetic Bragg scattering. The formation of a glassy ground state requires the existence of competing interactions. Any superexchange between pairs of localized-electron Mn^{4+} cations will be antiferromagnetic, but the nature of the Mn^{4+}−Ru^{4+} and Ru^{4+}−Ru^{4+} interactions will depend on the relative magnitude of the energy of the individual t_{2g} orbitals and the crystal field splitting which they experience. In the localized electron limit, in-plane Mn^{4+}−Ru^{4+} π superexchange involving the half-filled d_{xy} orbitals is expected to be antiferromagnetic, whereas the interactions involving the d_{xz} and d_{yz} orbitals will be ferromagnetic; both interactions will be antiferromagnetic in the case of Ru^{4+}−Ru^{4+} superexchange. However, as the energy levels broaden into bands and lose their atomic character, the latter interaction is likely to become ferromagnetic. The competing interactions needed to induce the formation of a spin-glass phase are therefore present, and their relative strength will vary as the magnitude of the octahedral distortion varies with temperature; we have shown previously[31] that small changes in crystal structure can have a large effect on the magnetic properties of $n = 1$ RP phases.

One possible interpretation of the magnetometry experiments performed on Sr_3MnRuO_7 is that extensive spin clustering occurs within the bilayers of the $n = 2$ RP structure below ~200 K; the lack of hysteresis suggests that the sample could be described as a superparamagnet in the temperature range $\sim 90 \leq T/K \leq 200$. The weak-field hysteresis apparent for $T < 90$ K marks the onset of irreversibility, perhaps associated with the development of antiferromagnetic intercluster interactions, and the local maximum in the ZFC susceptibility at 25 K can be taken to mark spin-glass freezing, again caused by the presence of competing interactions in a disordered cation arrangement. Com-

(29) Shaked, H.; Jorgensen, J. D.; Short, S.; Chamaissem, O.; Ikeda, S. I.; Maeno, Y. *Phys. Rev. B* **2000**, *62*, 8725.

(30) Shaked, H.; Jorgensen, J. D.; Chmaissem, O.; Ikeda, S.; Maeno, Y. *J. Solid State Chem.* **2000**, *154*, 361.

(31) Battle, P. D.; Bell, A. M. T.; Blundell, S. J.; Coldea, A. I.; Cussen, E. J.; Hardy, G. C.; Marshall, I. M.; Rosseinsky, M. J.; Steer, C. A. *J. Am. Chem. Soc.* **2001**, *123*, 7610.

parison of the data collected on the $n = 1$ and $n = 2$ samples supports the suggestion that the magnetization increase at relatively high temperatures, observed only in the latter, is a consequence of interactions within the perovskite blocks, whereas the transition at $\sim 20 \pm 5$ K, common to both samples, involves a 3D spin freezing. For both compositions, the maximum magnetization observed increases little on cooling from 50 to 5 K, although the field needed to induce the maximum effect does decrease on cooling. This suggests that magnetic clusters are well developed at 50 K, and it is the mean cluster size that increases on cooling, with spin-freezing occurring when a critical size is reached. The 1% perovskite impurity in the $n = 2$ sample could, if it were ferromagnetic with 1 μ_B per formula unit, account for the slight nonlinear field dependence of the magnetization at 150 K, but it could not account for the hysteresis observed at low temperatures.

The magnetic transition at 16 K appears to have no effect on the electrical resistance of the $n = 1$ phase, but that of the $n = 2$ phase drops by a factor of ~ 5 at the 25 K transition. Furthermore, the magnetoresistance is greatest at temperatures (50−75 K) slightly above this point. This can be taken as evidence that the ferromagnetic coupling between neighboring Mn^{4+} and Ru^{4+} cations plays a key role in driving the transition, the argument being similar to that used to explain the observation of CMR in ferromagnetic perovskite manganates at temperatures just above T_c. However, the presence of strong, competing antiferromagnetic interactions in the $n = 2$ composition described here leads to the formation of a spin-glass phase rather than a ferromagnetic ground state. The relative strength of these interactions will vary with temperature as the population of the d orbitals changes, with ferromagnetic coupling and the concentration of mobile electrons increasing as the population of the degenerate d_{xz} and d_{yz} orbitals increases on cooling, as described above. The absence of a decrease in resistivity at the glass transition temperature in the $n = 1$ case provides a fascinating contrast with the $n = 2$ material, and we are currently investigating these materials by μSR spectroscopy and ac magnetometry to understand this behavior, which is presumably controlled by the thickness of the perovskite blocks.

Acknowledgment. We are grateful to EPSRC, the ORS Award Scheme, and the University of Oxford for financial support. We thank T. Hansen and L. M. Murphy for experimental assistance at ILL Grenoble and SRS Daresbury, respectively.

CM021202S